Final Report

Contract DE-FG02-05ER84350

200 MW L-Band Annular Beam Klystron for Accelerators

Michael E. Read, Principal Investigator
Calabazas Creek Research Inc.
February 11, 2009

Table of Contents

Table of Contents ii
Introduction 1
Program Goal and Summary of Accomplishments 3
Accomplishments 3
Electron Gun 3
TRAK simulations 3
MIG gun simulation in 2D MAGIC 6
Gun Mechanical Design 7
RF structure 11
Modeling of the Input and Output Cavities Using MAGIC 15
Cold Testing 18
RF Structure Fabrication 19
Collector, output couplers, windows and loads 22
Collector 22
Output window 24
Water load 25
Solenoid 27
Conclusion 28
References 28

Introduction

This program was for the development of a 200 MW, 1.3 GHz, Annular Beam Klystron (ABK) for accelerator systems. An ABK provides lower impedance than a conventional klystron, making it possible to produce higher RF powers with lower voltages. With a higher power per unit, fewer klystrons would be required for a large accelerator. Lower voltage also simplifies and reduces the cost of the power supply system. Both features will significantly lower the cost of an RF system.

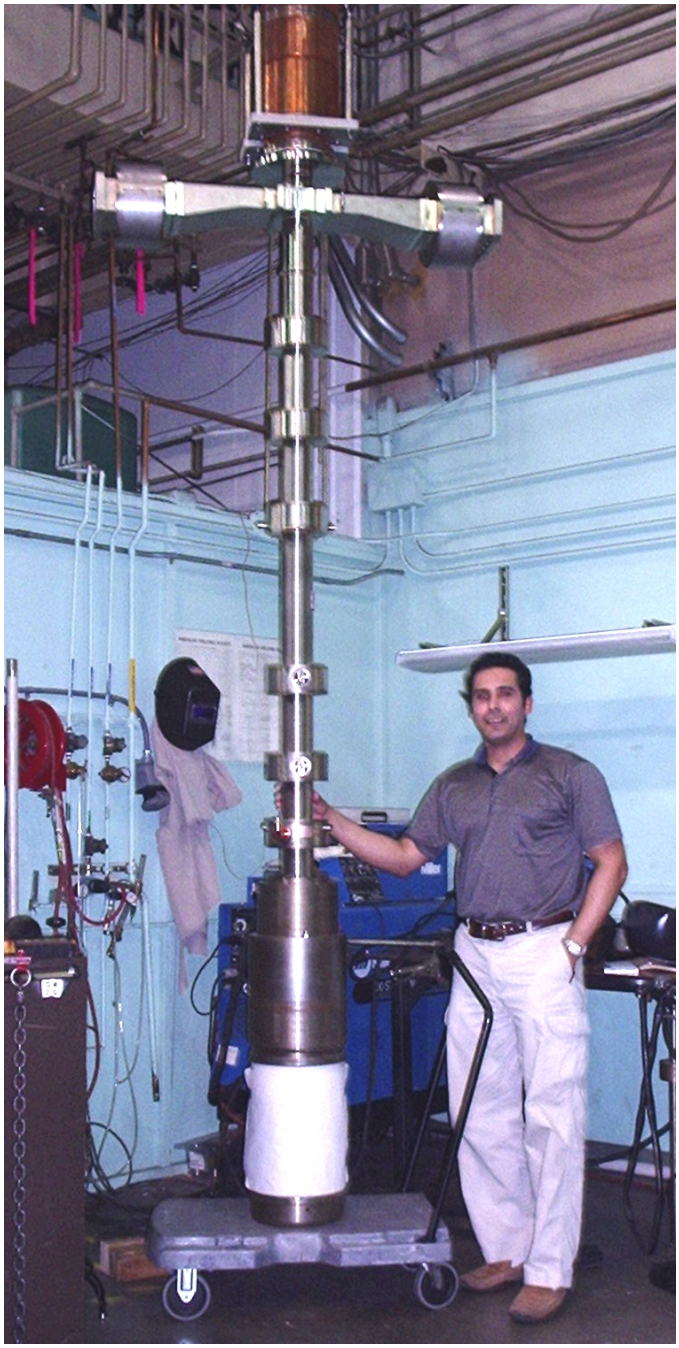

Figure 1. CCR Annular Beam Klystron, without the solenoid.

Several groups investigated ABKs for producing multi-gigawatt, short, microwave pulses for Department of Defense (DoD) applications. Their origin is the Relativistic Klystron Amplifier (RKA), first demonstrated by Friedman at the Naval Research Laboratory [1,2]. Friedman demonstrated a 6 GW source producing approximately 100 ns pulses. They obtained an efficiency of 50% for production of 3 GW pulses at 1.3 GHz. Researchers at Los Alamos National Laboratory (LANL) [3,4] and Mission Research Corporation (MRC) [5] pursued programs to demonstrate longer and repetitively pulsed devices. MRC achieved approximately 500 MW, 800 ns pulses in L-Band and another promising source at X-Band.

NRL and MRC used field emission cathodes, which are not compatible with longer pulses or significant repetition rates. In contrast, a 1 GW L-Band klystron at LANL included a thermionic cathode capable of high repetition rates. Through a carefully designed and simulated electron gun, the tube was expected to produce a 4 kA beam at 800 kV. Only a beam stick was fabricated in the LANL program, and testing was curtailed due to an open cathode heater.

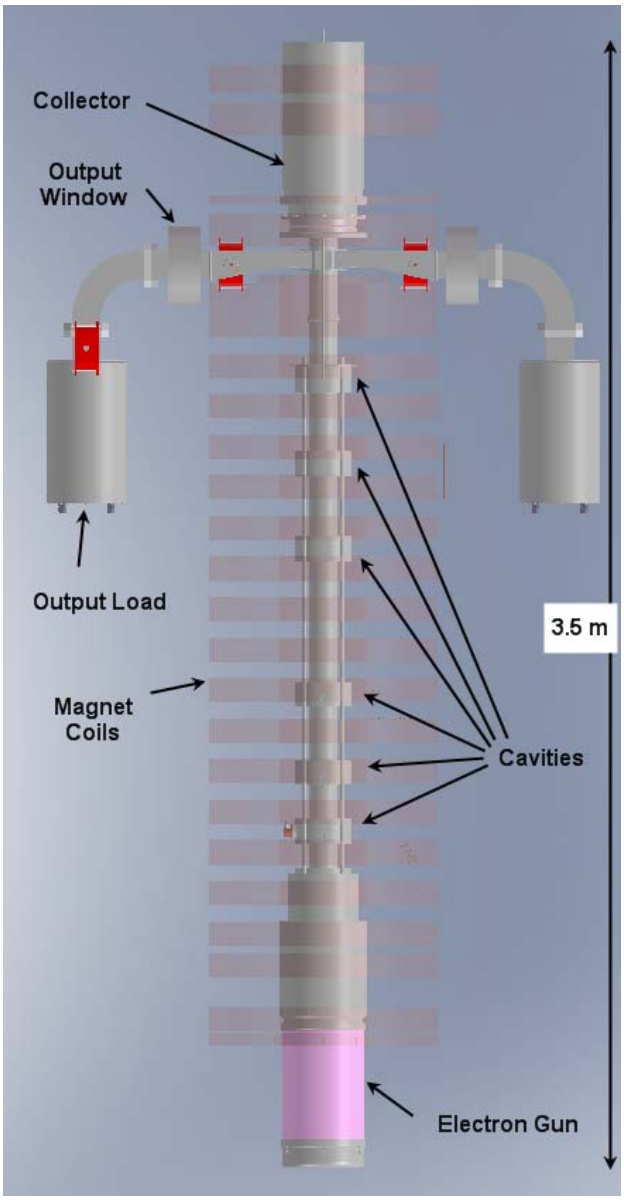

Figure 2. Solid model of the annular beam klystron. The tube is 3.5 meters long.

Table 1. Simulated parameters of the proposed ABK

Frequency	1.3 GHz
Power	200 MW
Efficiency	46%
Beam Voltage	475 kV
Beam Current	1100 A
Pulse Width	1 microsecond
Pulse Repetition Frequency	120 Hz

A power level of one GW is probably too high for accelerator applications, and 800 kV is definitely too high a voltage to be economically viable. CCR's device is designed to produce 200 MW with a beam voltage of 500 kV.

The CCR ABK is shown in Figure 1 and Figure 2. Salient features include the electron gun (1), input and buncher cavities (2) output cavity (3), output windows (4) and collector (5).

Output coupling is through two broadband high power vacuum ceramic windows operating in the TE_{10} mode in WR-650 waveguide located 180^{o} apart.

The electron gun is a Magnetron Injection Gun (MIG) with a conventional tungsten matrix emitter. This allows for microsecond-long pulses and high repetition rates required for accelerator applications. Although shallow angle MIG's can be subject to instabilities, extensive modeling by LANL and SLAC using DEMEOS [6] and a time domain simulation code, ISIS demonstrated stability of the original LANL design. Simulations by CCR also show stability for the proposed design.

The perveance of the proposed design is 3.4 micropervs. For a conventional design (using a solid beam), CCR obtained an efficiency of 37%, while 46% is predicted for the ABK. CCR analysis also determined that the RF field in the output cavity gap was only 159 kV/cm, a value much lower than possible with a solid electron beam.

Extensive simulations in Phase I predict the parameters shown in Table 1. These results indicate that a high efficiency, 200 MW, L-Band, ABK is feasible, and it was proposed that a 200 MW ABK be fabricated and tested in Phase II.

Program Goal and Summary of Accomplishments

The goal of the program was to complete the design, fabricate and test the klystron. The klystron was designed and the electron gun, circuit, input and output windows and collector were fabricated. After completion of these elements, it was determined that the available resources would not be adequate to complete fabrication of the solenoid, final assembly of the tube and testing. While it is normally CCR's policy to do everything possible to complete a project, in this case there had been a dramatic change in the market that made it unwise to expend internal funds. The ABK was originally intended as a source for the next generation collider. However, while the frequency was still appropriate, the requirement for the accelerator - the International Linear Collider - was for a 10 MW source with a 1.5 ms pulse length. While the 200 MW device was still relevant to test the concept of the ABK, it was clear that the cost of completing that device was unjustifiably high. Accordingly, the program was terminated.

Accomplishments

Electron Gun

A Magnetron Injection Gun is used to produce the annular beam. This gives the required beam density with a cathode loading of 7.8 A/cm^2. To insure stability, the gun is run temperature-limited. The gun was extensively simulated in Phase I. In Phase II, the electron gun optics were confirmed using additional simulations in TRAK and the particle in cell (PIC) code MAGIC. The MAGIC simulations showed that the gun achieves equilibrium smoothly, eliminating concerns regarding stability.

TRAK simulations

The trajectories from the final TRAK simulation are shown in Figure 3 and Figure 4. The magnetic field used in the simulations is shown in Figure 5.

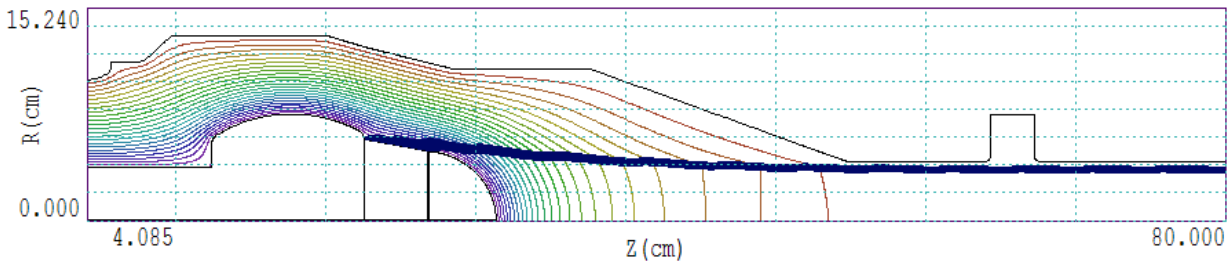

Figure 3. Trajectories from the final TRAK simulation.

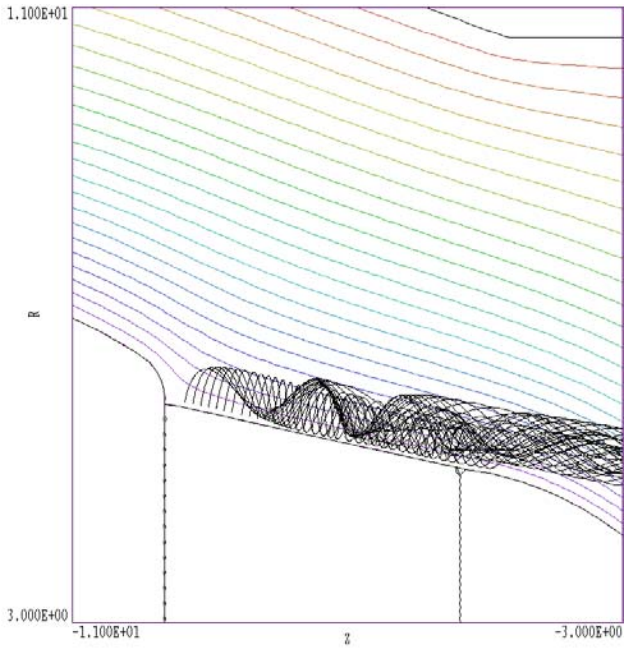

Figure 4. Detail of the trajectories near the cathode.

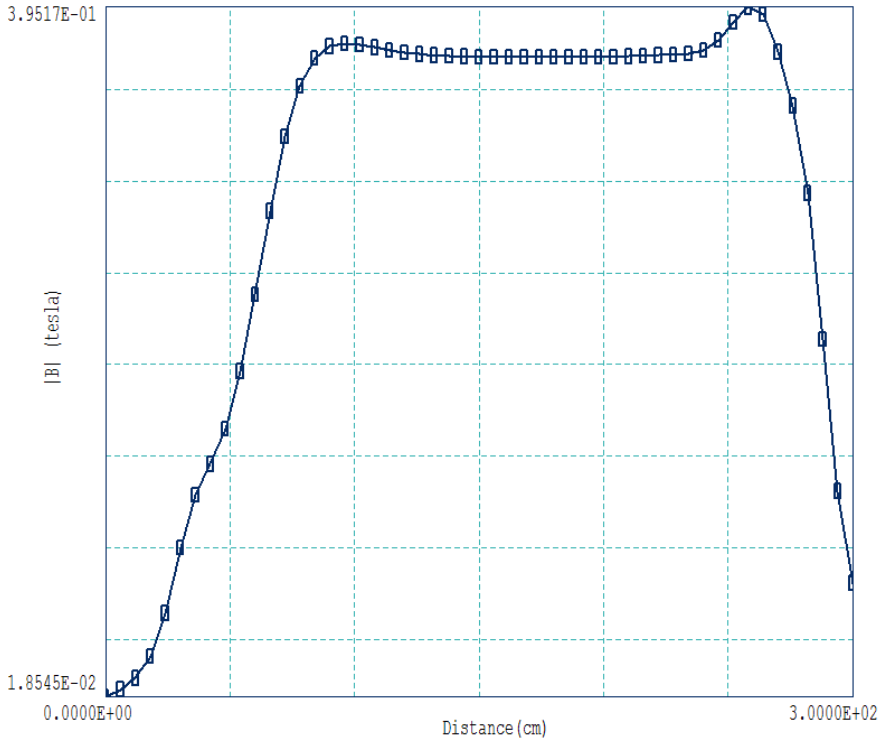

Figure 5. Magnetic field, on axis, used in the gun simulations. The origin is 25 cm to the left of the origin shown in Figure 3.

One of the undesirable features of the MIG is motion perpendicular to the magnetic field. The energy associated with this motion cannot be transferred to RF energy, and thus it reduces the efficiency. Accordingly, an effort was made to minimize perpendicular electron motion. The perpendicular velocity is proportional to the electric field at the cathode and to the cathode magnetic field to the -3/2 power. Since space charge imposes a lower limit on the electric field, the primary approach was to minimize the compression ratio. This is bounded by the cathode loading. The parameters shown in reflect a balance between the perpendicular energy and cathode loading. The perpendicular energy of the individual beam trajectories is shown in Figure 6.

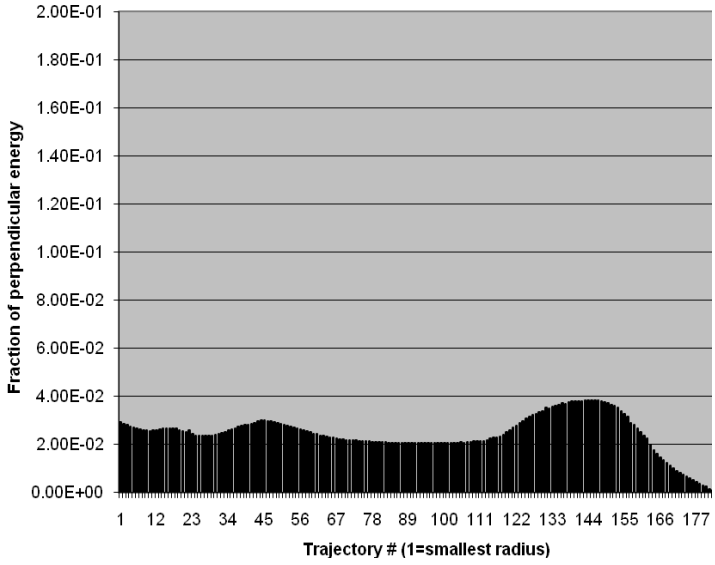

Figure 6. Fraction of electron energy transverse to the axis for the fully compressed beam.

The gun and beam parameters are summarized in Table 2.

Table 2. Beam parameters.

Voltage	500 kV
Current	1100 A
Cathode loading	7.8 A/cm^2
Cathode radius (average)	5.43 cm
Beam radius Inner Outer	 3.40 cm 3.84 cm
Magnetic field at cathode in RF structure	 1360 G 3700 G
Potential depression in RF structure region	17 kV
Average fraction of energy in perpendicular motion	4.6%

MIG gun simulation in 2D MAGIC

Because of the long slant length and high current density, there was some concern as to the stability of the emission. The PIC code MAGIC 2D was used to check the stability. The geometry and magnetic field were the same as those used in the TRAK simulations. The gun geometry is shown in Figure 7The beam behavior is presented in the following figures.

As shown in Figure 8, a rise time of 5 ns was used in the simulations. Capacitive effects resulted in an overswing, but the voltage reached an equilibrium of 500kV at 20 ns. Figure 9 shows that the 1100A beam becomes stable after a few nanoseconds. Equilibrium was reached more quickly than the voltage because the emission is temperature limited.

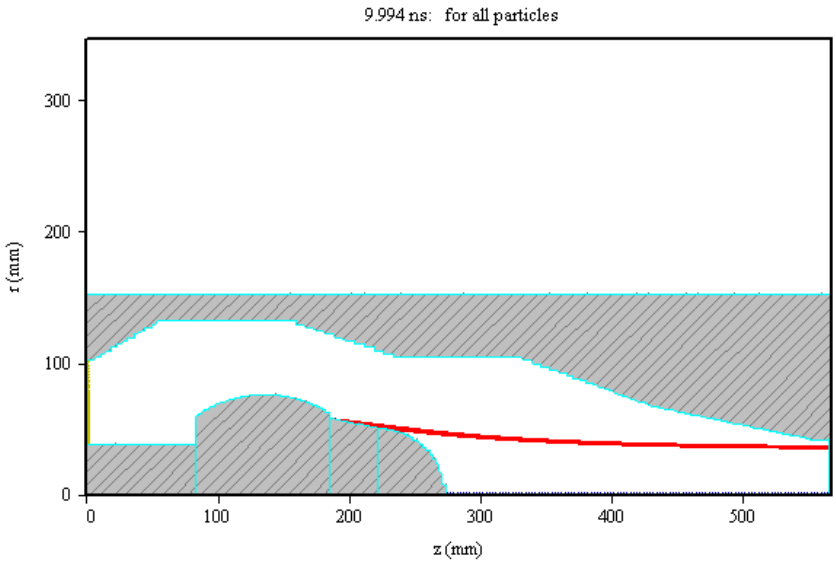

Figure 7. MIG gun and trajectories as modeled using MAGIC.

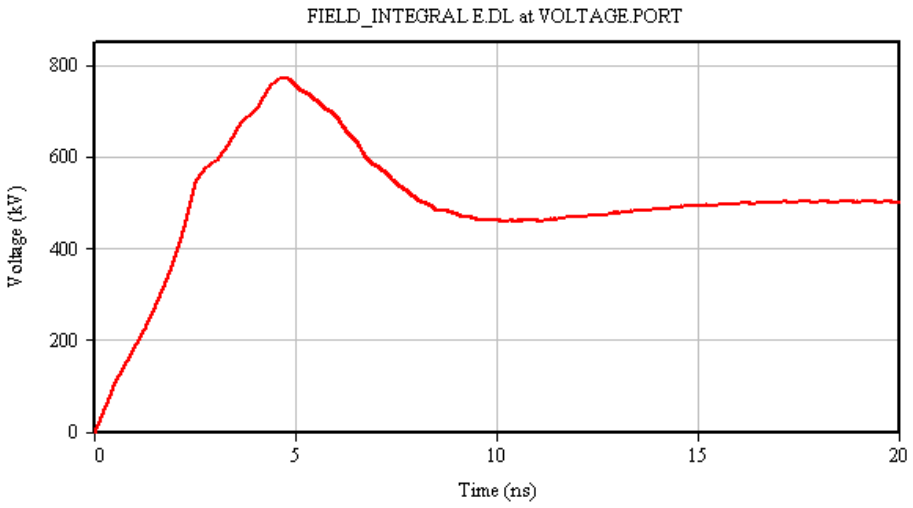

Figure 8. Voltage from the anode to cathode.

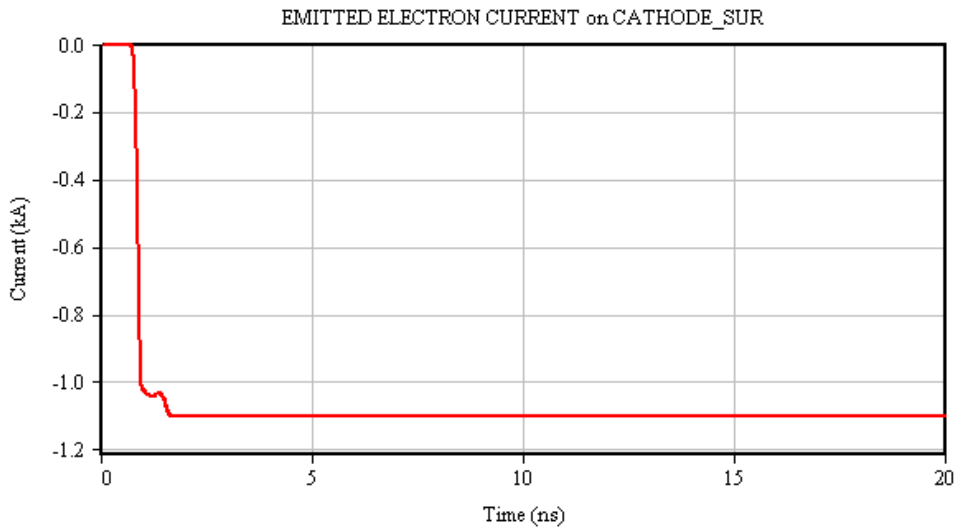

Figure 9. Beam current as a function of time.

Gun Mechanical Design

The gun mechanical design is shown in Figure 10. The completed gun is shown in Figure 11, and the emitter in a bell jar is shown in Figure 12.

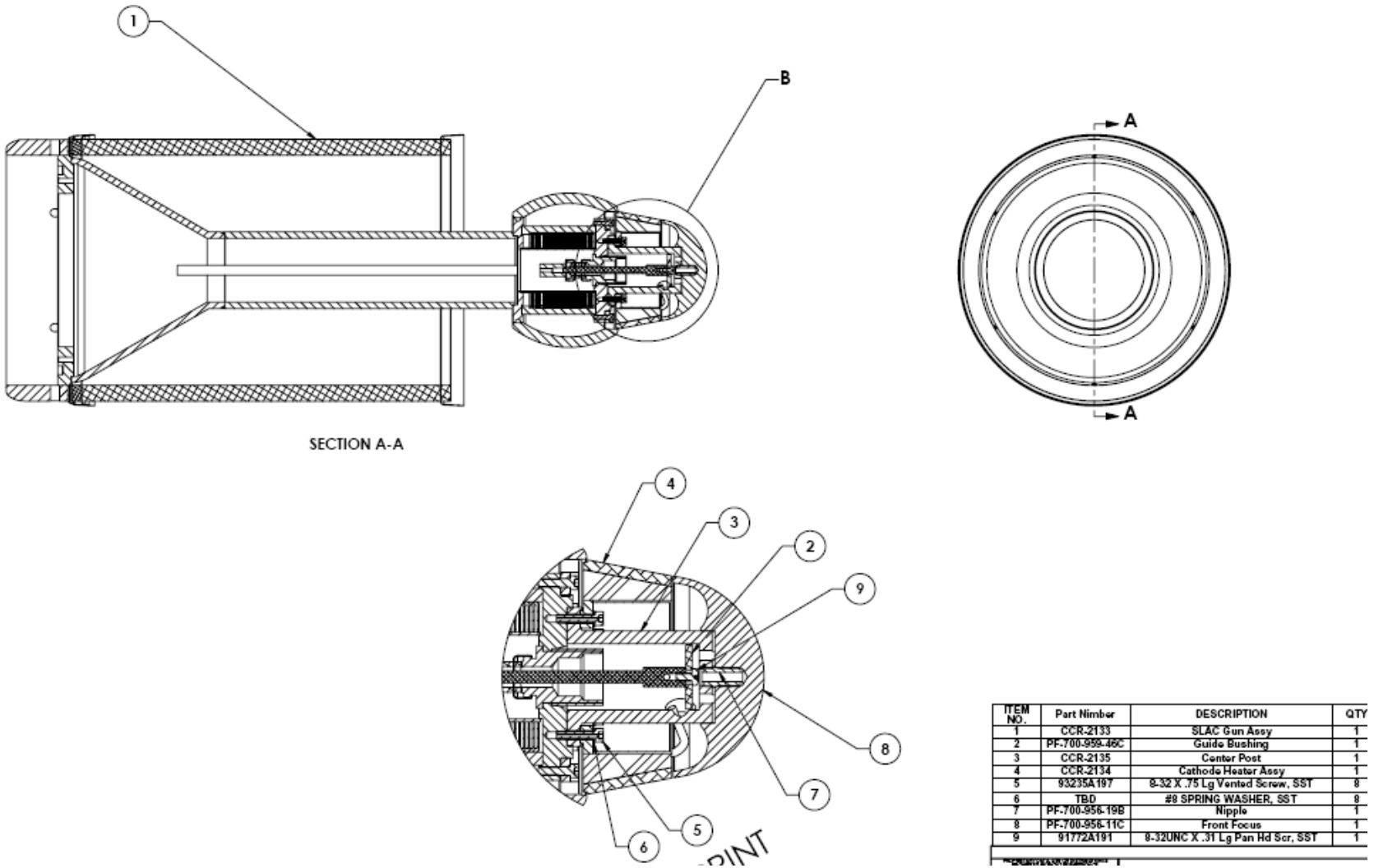

ITEM NO.	Part Nimber	DESCRIPTION	QTY
1	CCR-2133	SLAC Gun Assy	1
2	PF-700-959-46C	Guide Bushing	1
3	CCR-2135	Center Post	1
4	CCR-2134	Cathode Heater Assy	1
5	93235A197	8-32 X .75 Lg Vented Screw, SST	8
6	TBD	#8 SPRING WASHER, SST	8
7	PF-700-956-19B	Nipple	1
8	PF-700-956-11C	Front Focus	1
9	91772A191	8-32UNC X .31 Lg Pan Hd Scr, SST	1

Figure 10. Gun design.

Figure 11. The electron gun.

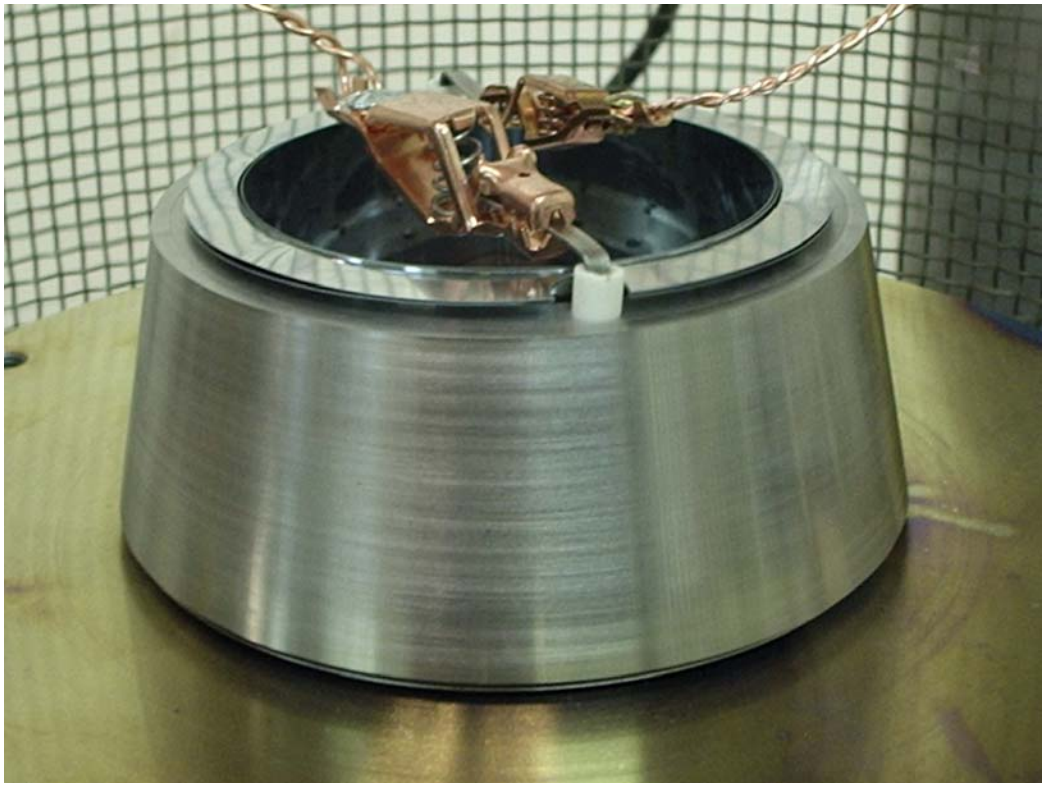

Figure 12. Emitter for the ABK.

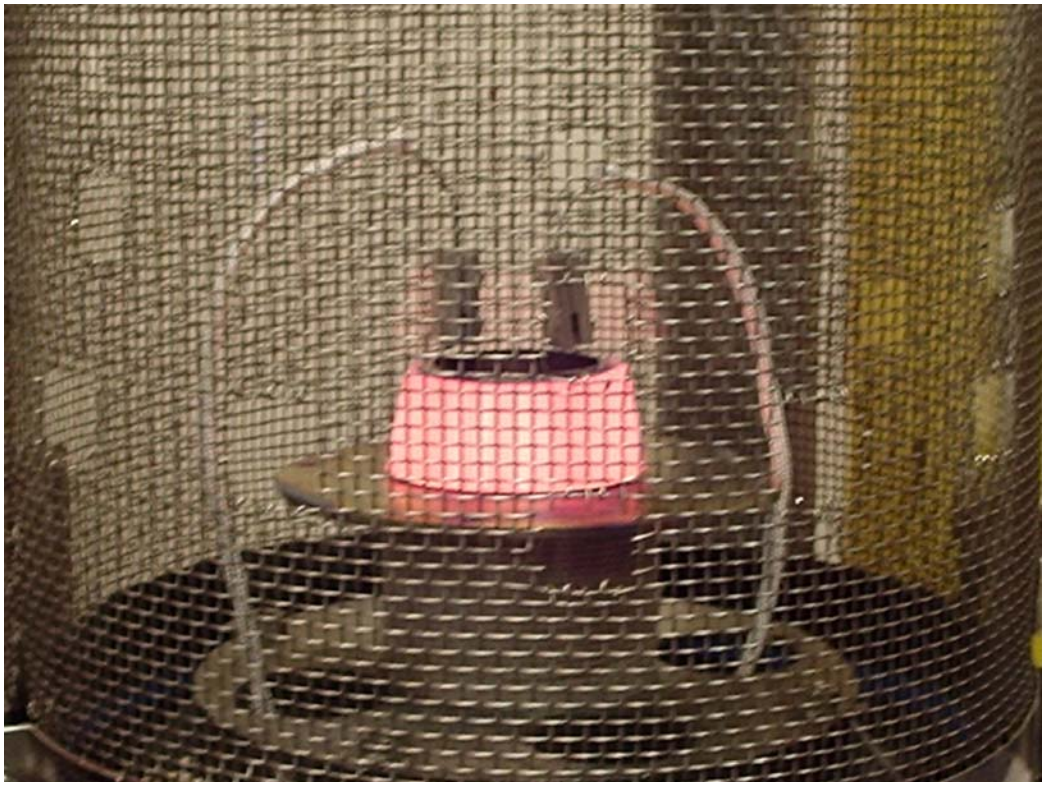

Figure 13. Emitter in a bell jar for thermal testing.

RF structure

Several views of the RF interaction circuit consisting of 7 cavities are shown in Figure 14. The circuit consists of an input cavity, 2 gain cavities, 3 penultimate cavities tuned above the center frequency for efficiency enhancement and an elliptically shaped output cavity loaded with 2 tapered waveguides located opposite diametrically. The loaded output cavity was designed using MAGIC to equalize the 2 radial electric fields, E_x and E_y. Capacitive tuners were employed for the first 4 cavities for fine tuning during final testing.

Final cavity parameters and the axial positioning of the 7 cavities are listed in Table 3. Final cavity parameters.

A cross section of a typical cavity is shown in Figure 15. This is referred to as a hybrid cavity because it has only one reentrant drift tube. Normal klystron cavities employ two reentrant drift tubes to concentrate the electric field. We employ this hybrid cavity because of its relative mechanical robustness, in particular, the downstream nose will not detune the cavity in the event of beam interception. The shunt impedance of the hybrid cavity is reduced slightly from that obtained from a double reentrant cavity.

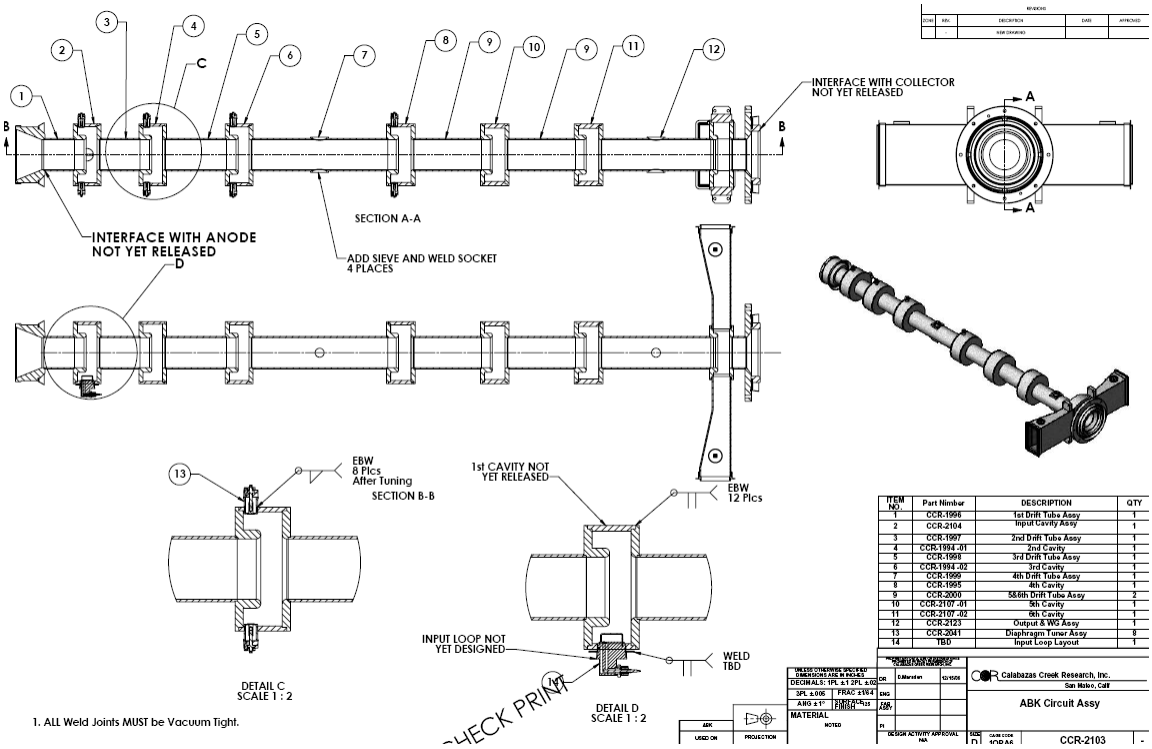

ITEM NO.	Part Number	DESCRIPTION	QTY
1	CCR-1996	1st Drift Tube Assy	1
2	CCR-2104	Input Cavity Assy	1
3	CCR-1997	2nd Drift Tube Assy	1
4	CCR-1994 -01	2nd Cavity	1
5	CCR-1998	3rd Drift Tube Assy	1
6	CCR-1994 -02	3rd Cavity	1
7	CCR-1999	4th Drift Tube Assy	1
8	CCR-1995	4th Cavity	1
9	CCR-2000	5&6th Drift Tube Assy	2
10	CCR-2107 -01	5th Cavity	1
11	CCR-2107 -02	6th Cavity	1
12	CCR-2123	Output & WG Assy	1
13	CCR-2041	Diaphragm Tuner Assy	9
14	TBD	Input Loop Layout	1

Figure 14. RF circuit for the 200 MW ABK

Table 3. Final cavity parameters

Cavity	Center of Gap Position (m)	Superfish Calculation (Q's are unloaded)			Cold Test Measurements	
		Frequency (MHz)	Q	R/Q	Frequency (MHz)	Loaded Q
1	0.1	1300	2264	80	1304	130
2	0.285	1290	2282	80	1285	1736
3	0.529	1325	2223	81.5	1326	1326
4	0.984	1379	2419	96.6	1381	1725
5	1.294	1449	2306	101	1451	2501
6	1.514	1475	2265	103.5	1477	2308
7	1.884	1305	2778	93.9	1301	11

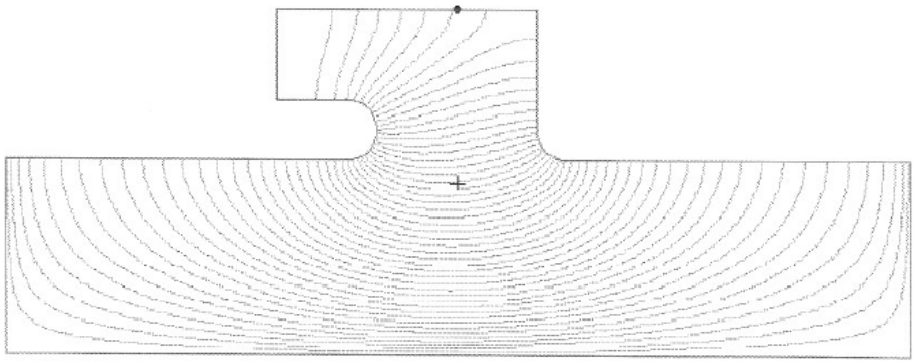

Figure 15. Typical cavity shape. This is called a hybrid cavity because it has only one re-entrant nose.

KLSC, our in-house klystron large signal code was used to simulate and optimize the efficiency of this 7 cavity circuit. The hollow electron beam consisting of 8 rings traversing the 7 cavity circuit is shown in Figure 16. Note the relative flatness of the this hollow electron beam, i.e., the beam is almost totally axially modulated as opposed to a solid electron beam which exhibits both axial and radial modulation. The flat axial magnet field was 3700 Gauss. The maximum efficiency obtained was 50.8% with no electrons reflected from the output cavity gap.

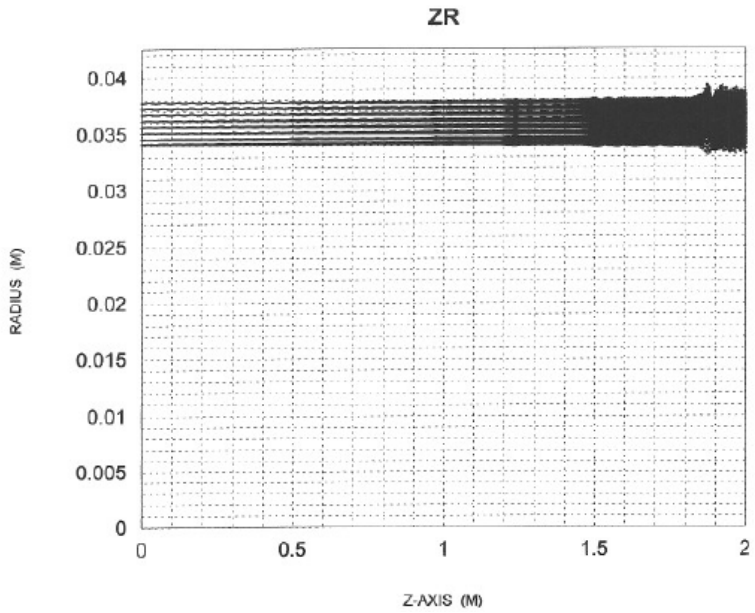

Figure 16. The Electron Beam Consisting of 8 Concentric Rings Traversing the Circuit.

Axial beam velocity as Beta (v/c) versus axial distance is plotted in Figure 17 and radial beam velocity as Beta in plotted in Figure 18. In Figure 17, the initial velocity is 0.82 corresponding to the initial beam voltage of 475 kV. In comparing the two velocities, note that the axial velocity at Z = 1.9 M decreases from Beta = 0.9 to approximately zero while the radial velocity varies between +.15 to -.15. This comparison indicates the dominant axial modulation of the hollow beam.

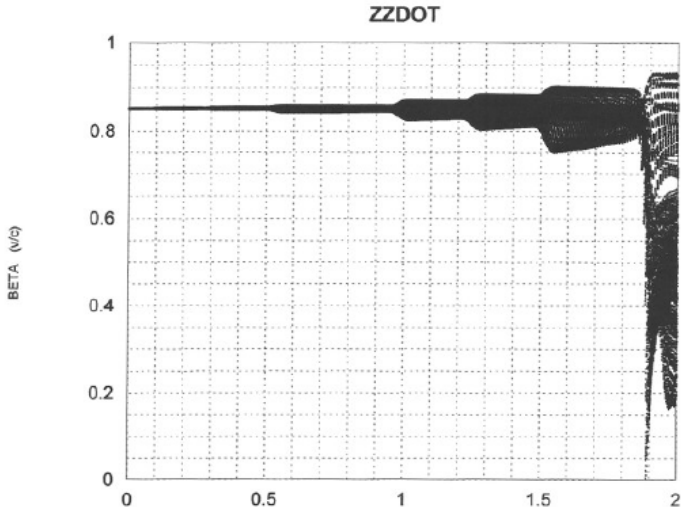

Figure 17. Betaz versus Z.

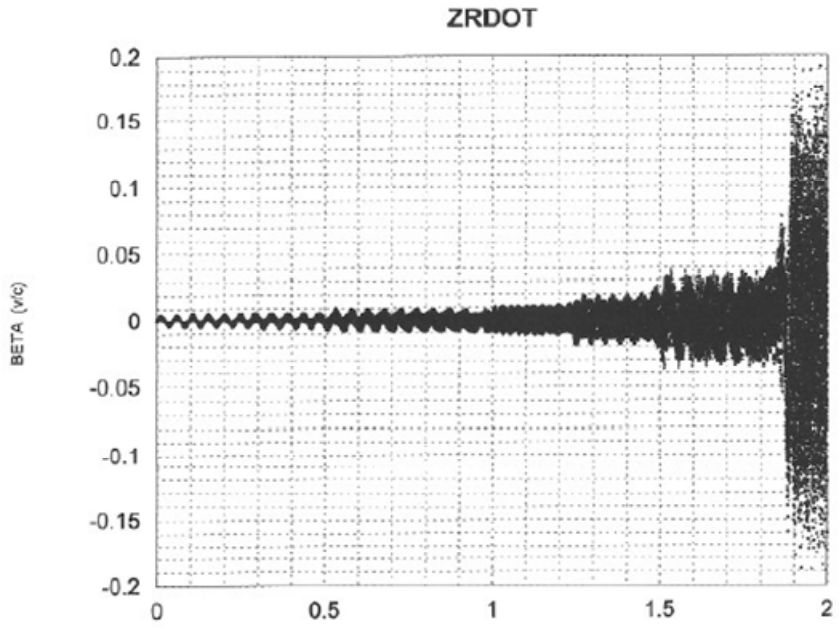

Figure 18. Radial velocity versus Z.

Modeling of the Input and Output Cavities Using MAGIC

The 3D particle-in-cell code MAGIC was used to model the input and output cavities. The input cavity was loop-coupled, and is shown in Figure 19 and Figure 20. Contour plots of the RF fields are shown in Figure 21 through Figure 23.

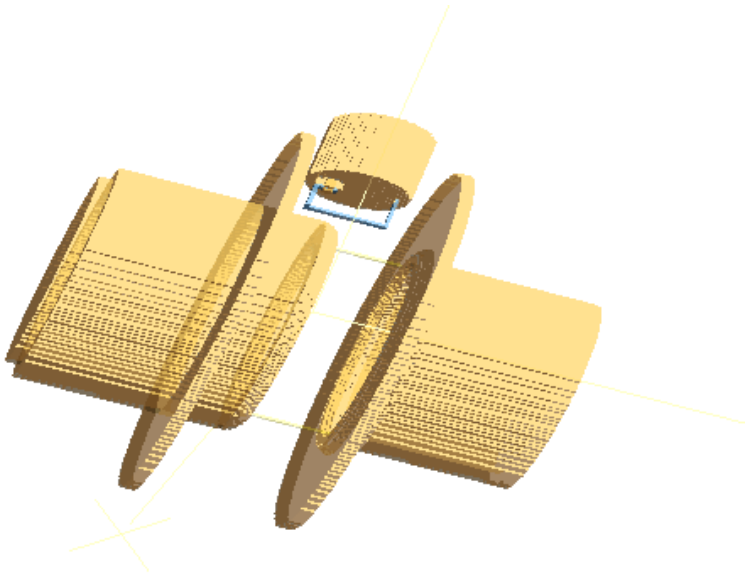

Figure 19. Geometry of the input cavity, as modeled using MAGIC 3 D.

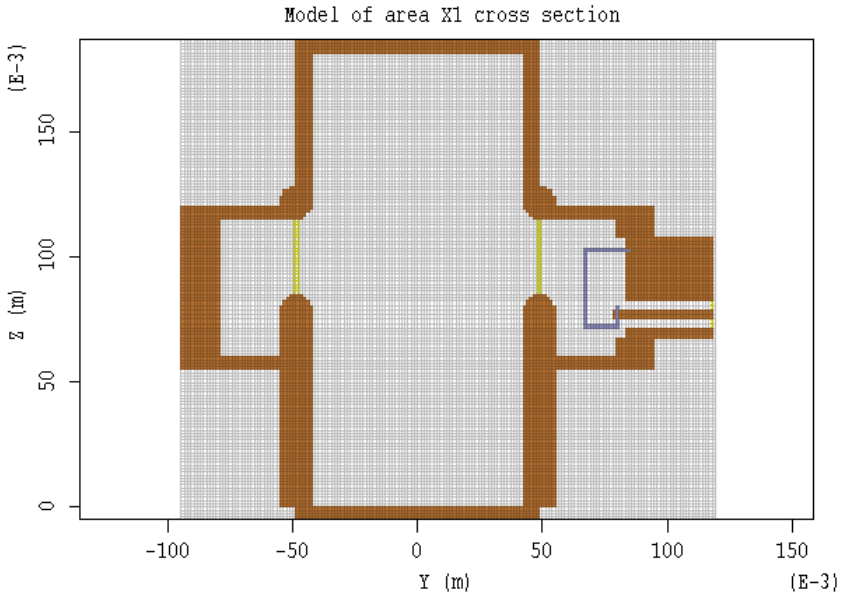

Figure 20. YZ cross section of the input cavity.

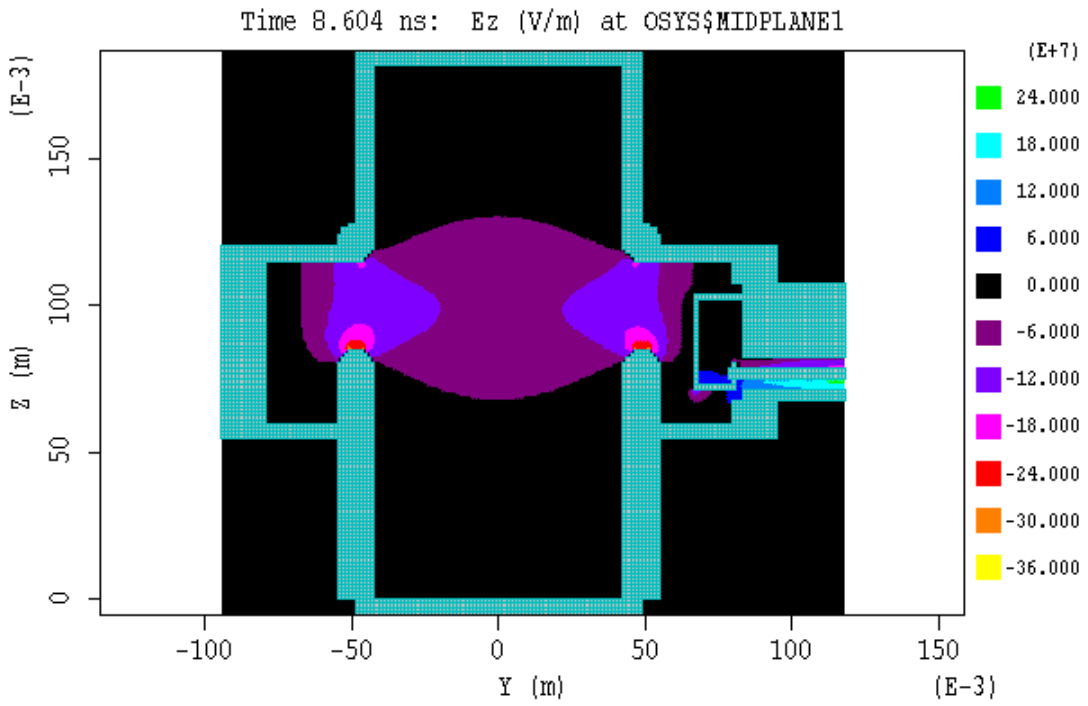

Figure 21. Ez contour plot at y-z plane at x=0

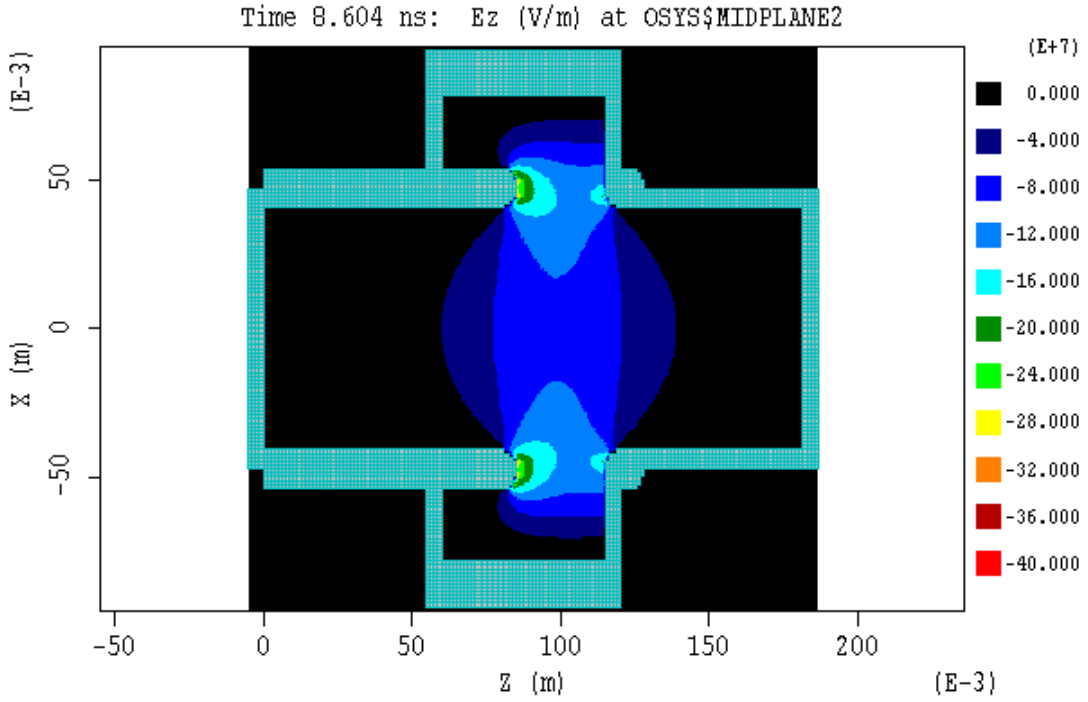

Figure 22. Ez contour plot at x-z plane at y=0

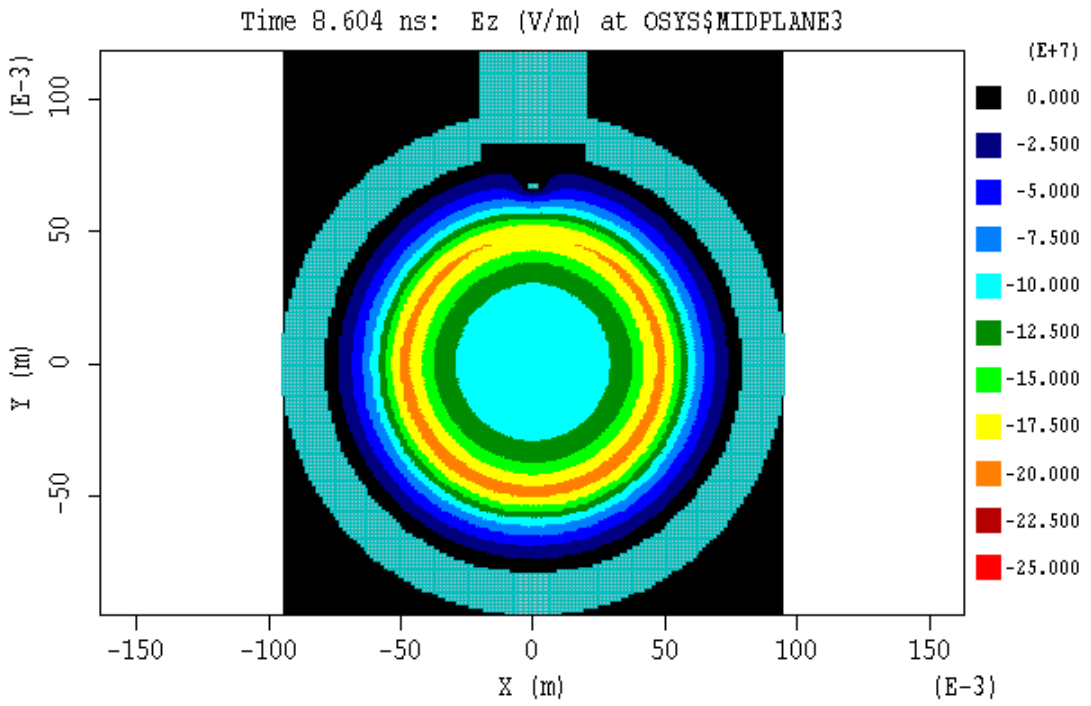

Figure 23. Ez contour plot at x-y plot at the gap center

The resonant frequency was 1301 MHz and the Q, calculated using the decay time of the field, was 146. Because of the very finite mesh in MAGIC, there was some concern as to the accuracy of the calculations. However, when the loop was removed, reducing the geometry to that which could be modeled using Superfish, the resonant frequencies agree to within 4 Hz.

The output cavity was iris coupled, and had an elliptical cross section. The cavity and the axial electric field, as modeled using MAGIC 3D are shown in Figure 24 and Figure 25. The resonant frequency and loaded Q were 1306 MHz and 11.2, respectively.

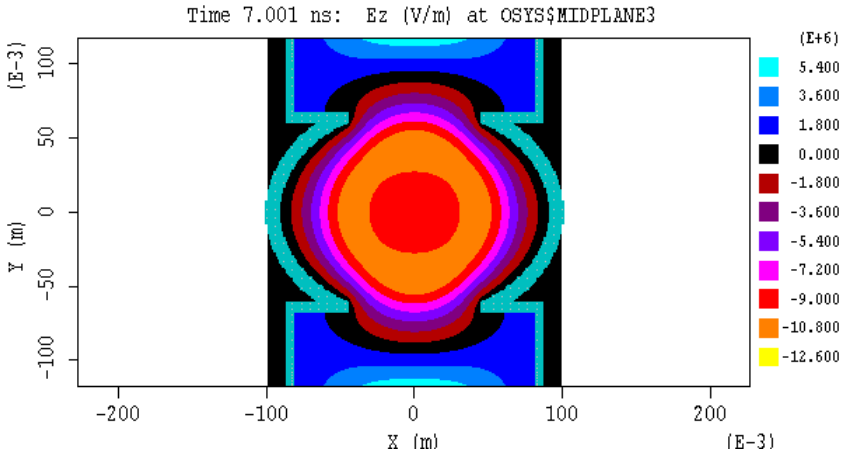

Figure 24. XY cross section of the output cavity, showing contours of E_z.

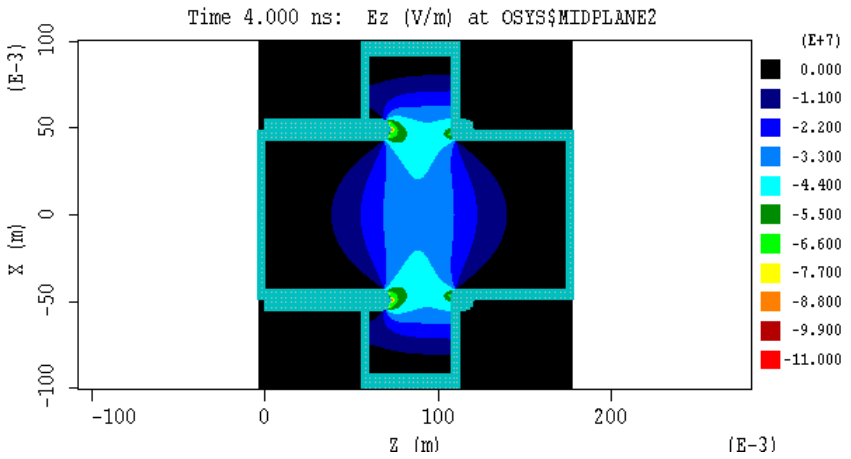

Figure 25. XZ cross section of the output cavity, showing contours of E_z.

Cold Testing

All of the cavities were cold tested to determine the resonant frequencies and Q's. Measurements were made before final assembly, allowing for adjustment of the dimensions to get the desired performance. Measurements for all but the output cavity were made with a scalar network analyzer. Because of the low Q, the output cavity Q was measured using a vector network analyzer and specialized software. Using measurement by reflection, the resonant frequency was 1.328 GHz, and the Q was 19. With the quartz rod perturbation technique, generally considered to be more reliable, the resonant frequency and Q were 1.340 +/- 0.002 GHz and 11.15 +/- 0.35, respectively. This is in good agreement with the MAGIC simulations. Results of the final cold tests are summarized in

Cavity	Center of Gap Position (m)	Superfish Calculation (Q's are unloaded)			Cold Test Measurements	
		Frequency (MHz)	Q	R/Q	Frequency (MHz)	Loaded Q
1	0.1	1300	2264	80	1304	130
2	0.285	1290	2282	80	1285	1736
3	0.529	1325	2223	81.5	1326	1326
4	0.984	1379	2419	96.6	1381	1725
5	1.294	1449	2306	101	1451	2501
6	1.514	1475	2265	103.5	1477	2308
7	1.884	1305	2778	93.9	1301	11

.

RF Structure Fabrication

A solid model of the RF section is shown in Figure 26. All but the output cavity were fabricated from stainless steel with the sidewalls copper plated Using stainless steel allowed the cavities to be welded together. Given the length of the structure, this was much easier than brazing. The structure is shown in Figure 27 through Figure 29.

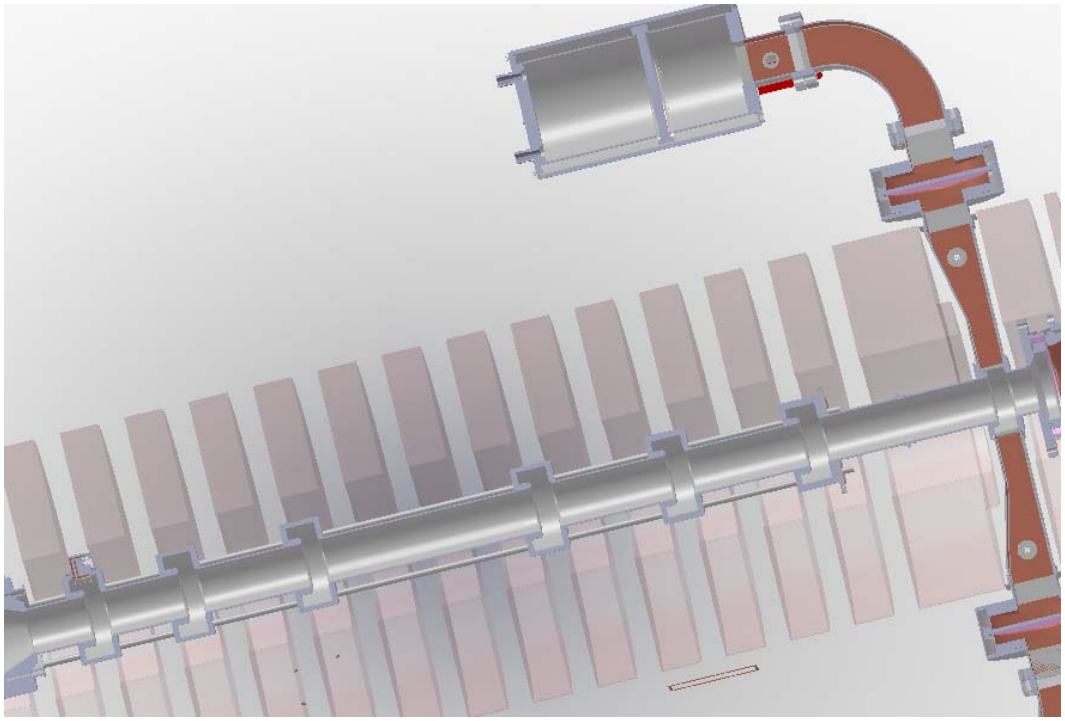

Figure 26. Solid model of the RF structure.

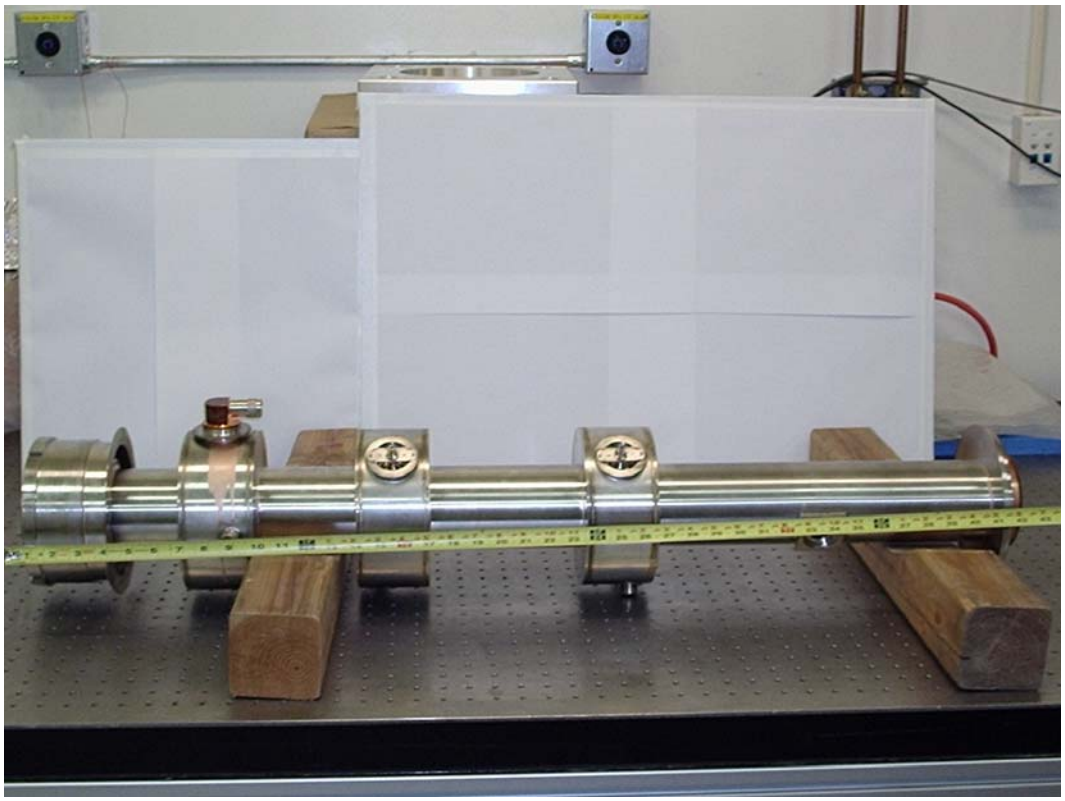

Figure 27. Anode and cavities 1 (input) 2, and 3.

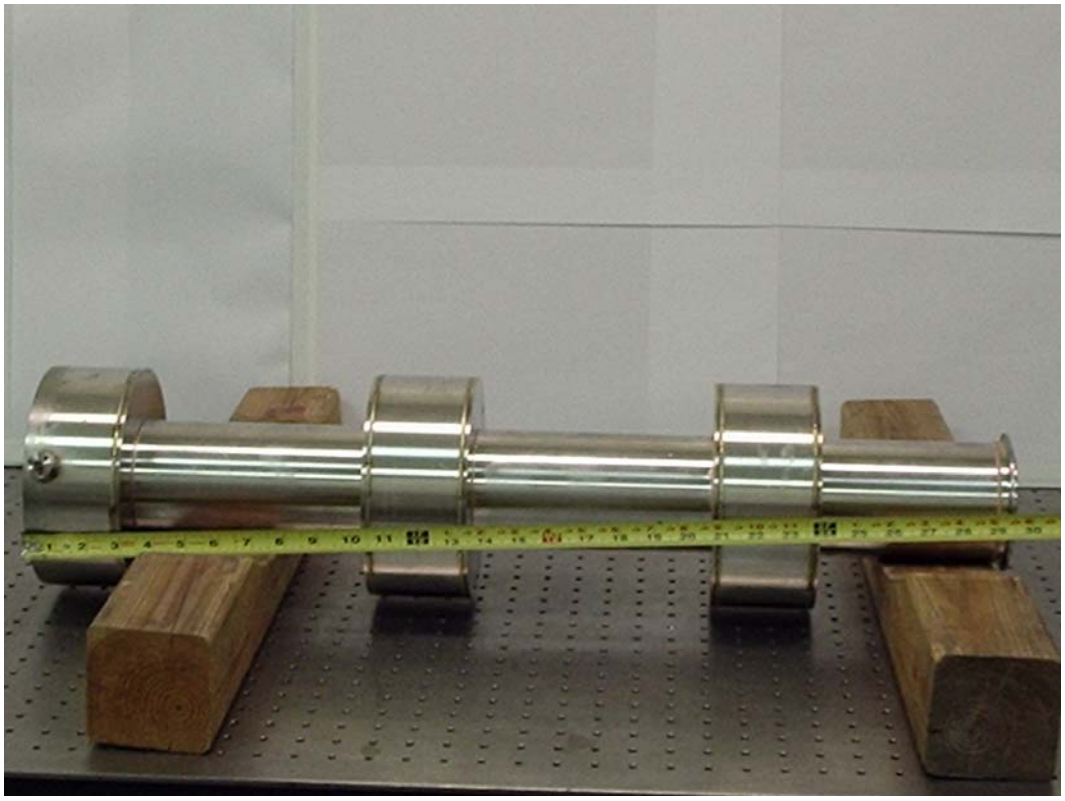

Figure 28. Cavities 4,5 and 6.

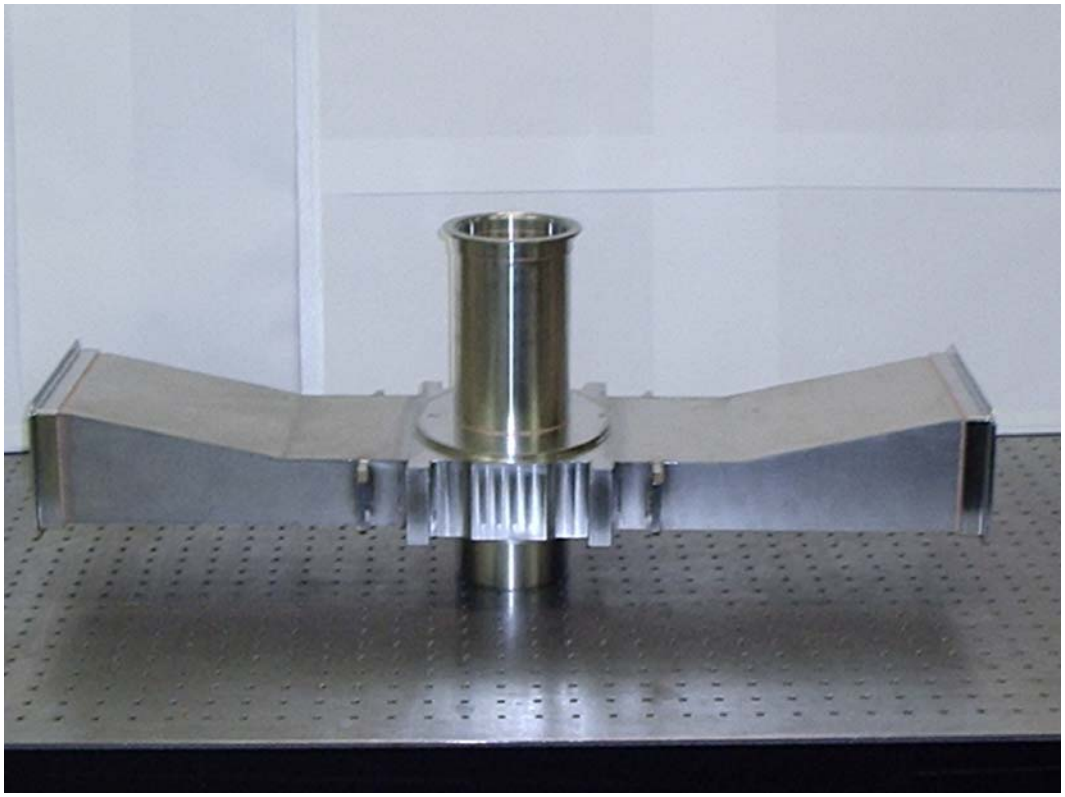

Figure 29. Output cavity with output waveguides.

Collector, output couplers, windows and loads

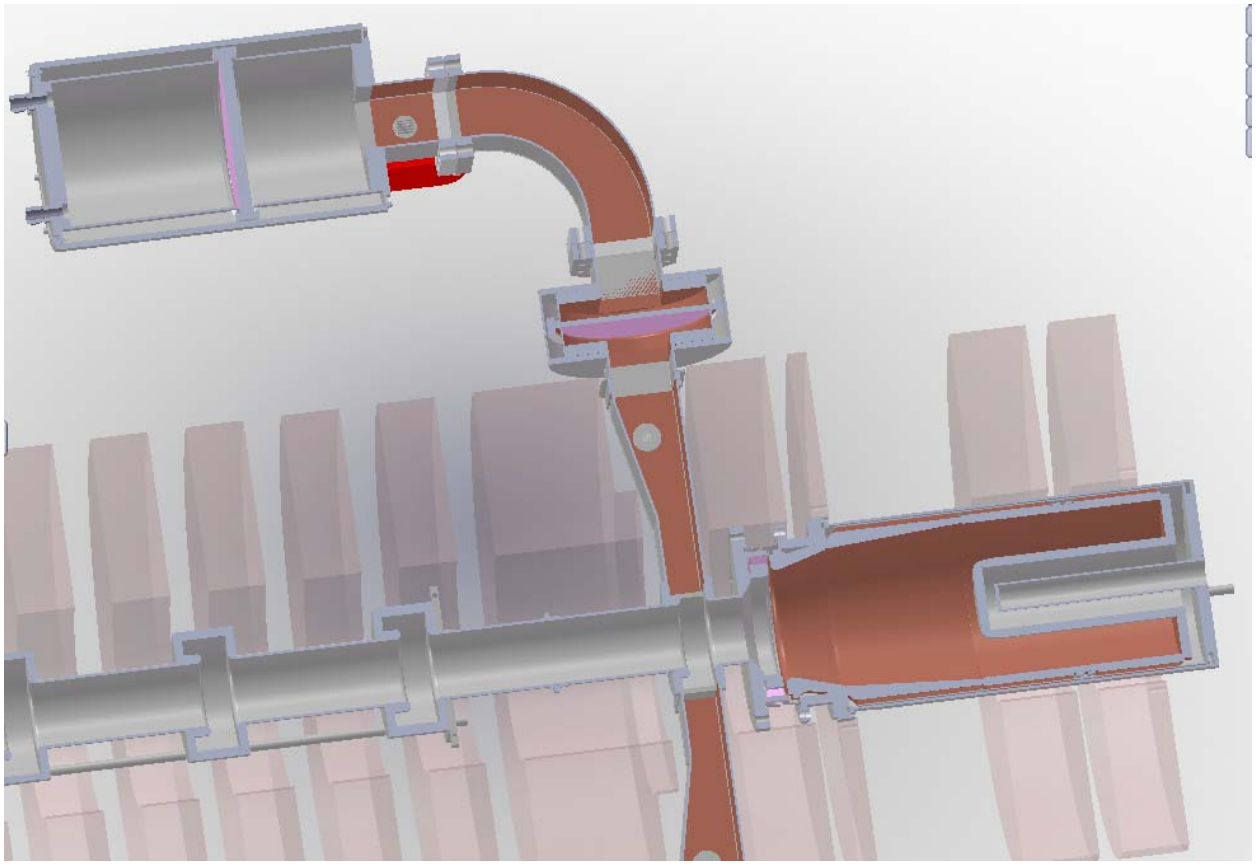

Figure 30. Output coupler, collector and water load.

Collector

The collector and beam trajectories are shown in Figure 31. The initial particle distribution was included the effects of the RF, and was generated by KLSC.

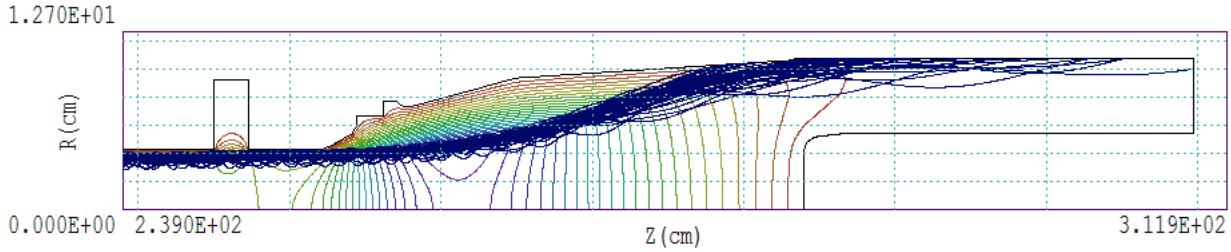

Figure 31. Collector trajectories with RF.

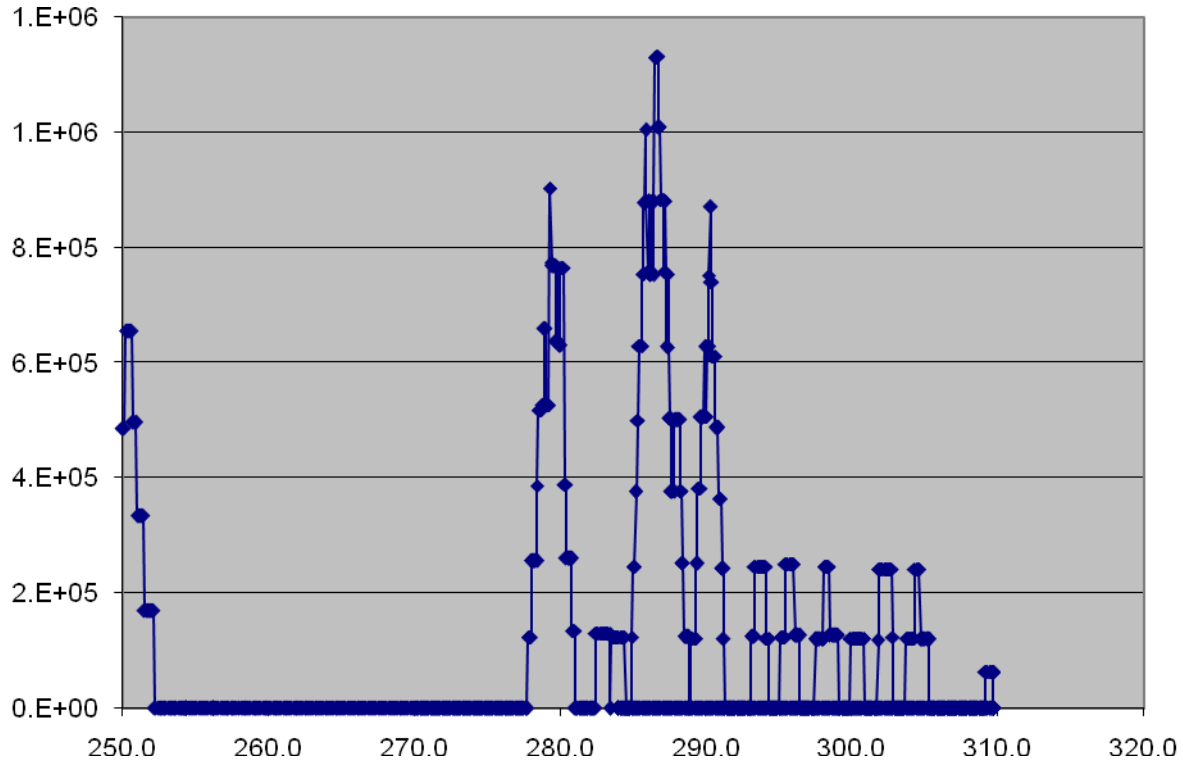

Figure 32. Collector power density with the trajectories of Figure 31.

Figure 33, Collector.

Output window

One of the two output windows is shown in Figure 34. As shown in Figure 35, the measured VSWR was 1.095. This was fully acceptable

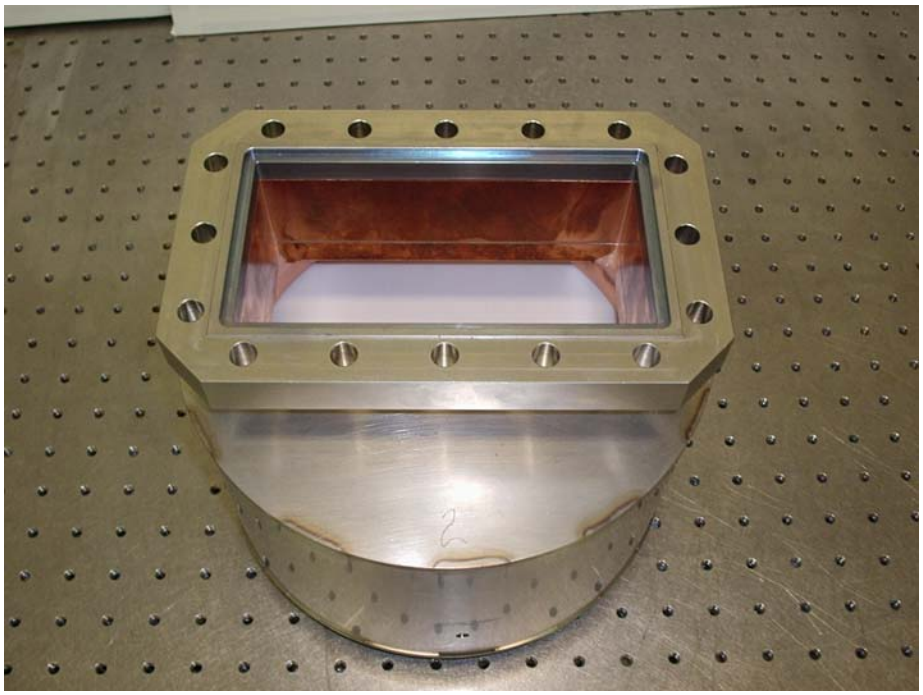

Figure 34. One of the two output windows.

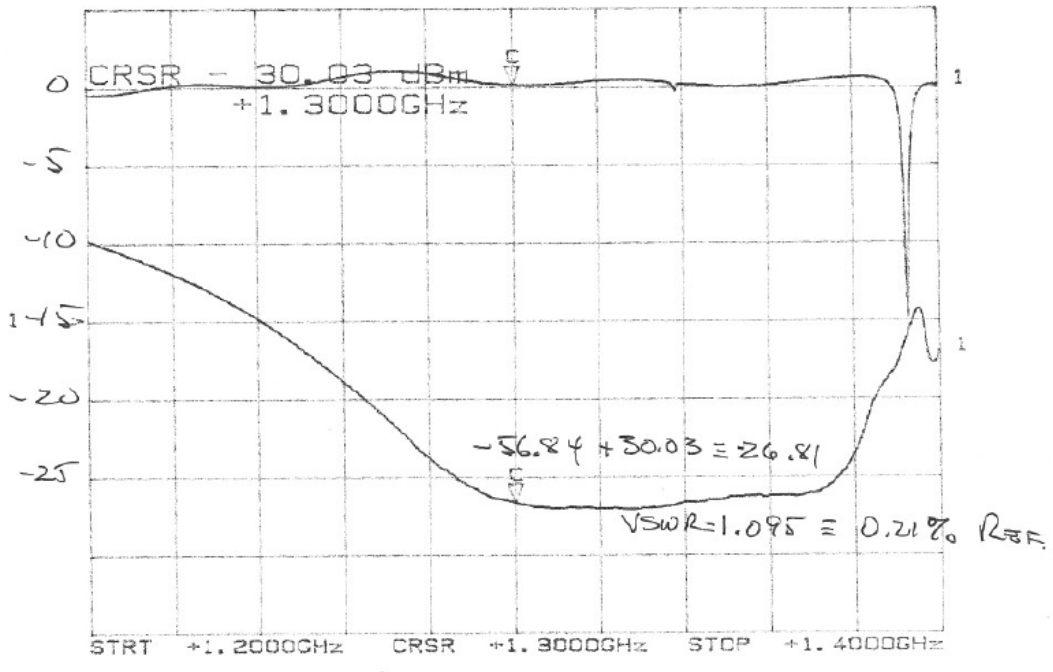

Figure 35. S11 for output window #1.

Water load

One of the two water loads is shown in Figure 36. Measurements of the reflection from the load, with the water at room temperature and at operating temperature are shown in Figure 37 and Figure 38, respectively. The VSWR is acceptably low for both conditions.

Figure 36. One of the two water loads.

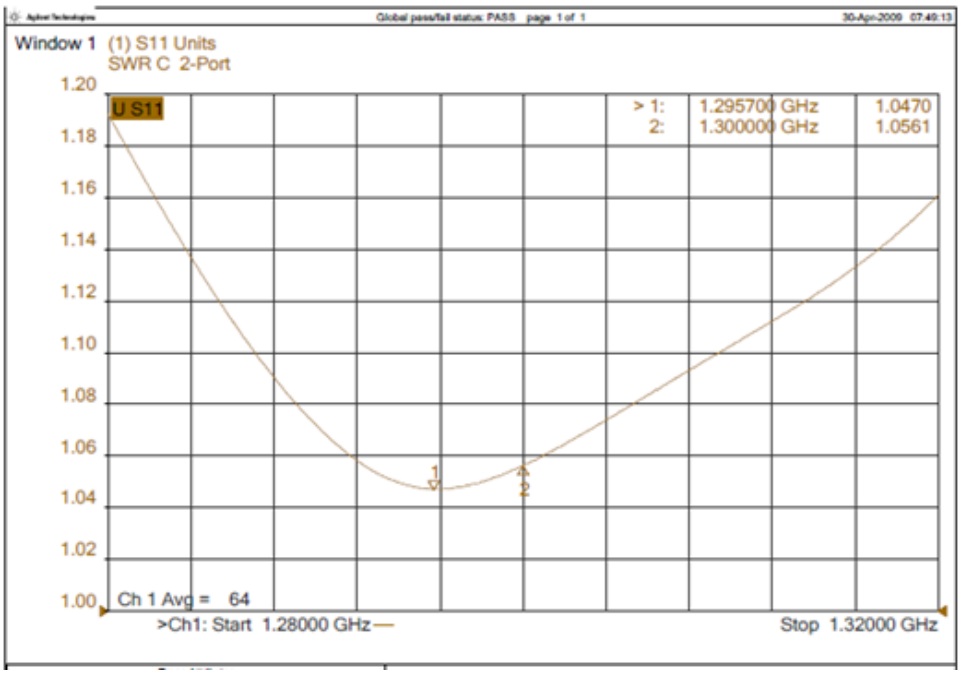

Figure 37. Water load VSWR with the load at room temperature.

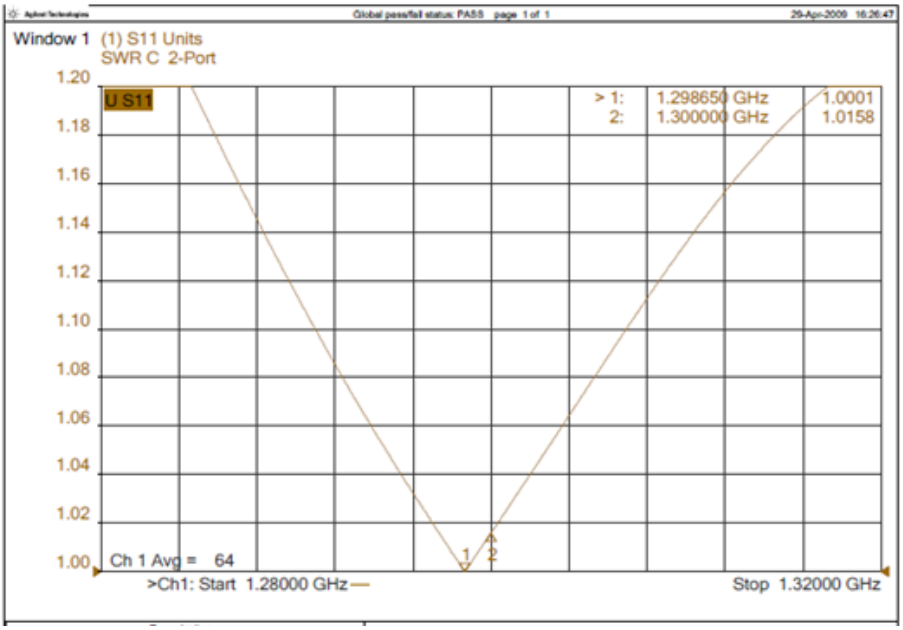

Figure 38. Water load VSWR with the load at the operating temperature.

Solenoid

The final design of the solenoid is shown in Figure 39. The solenoid consisted of multiple pancake coils with spacings for the input and output couplers, and access to tuning mechanisms. Because the program was terminated, the coils were not completed.

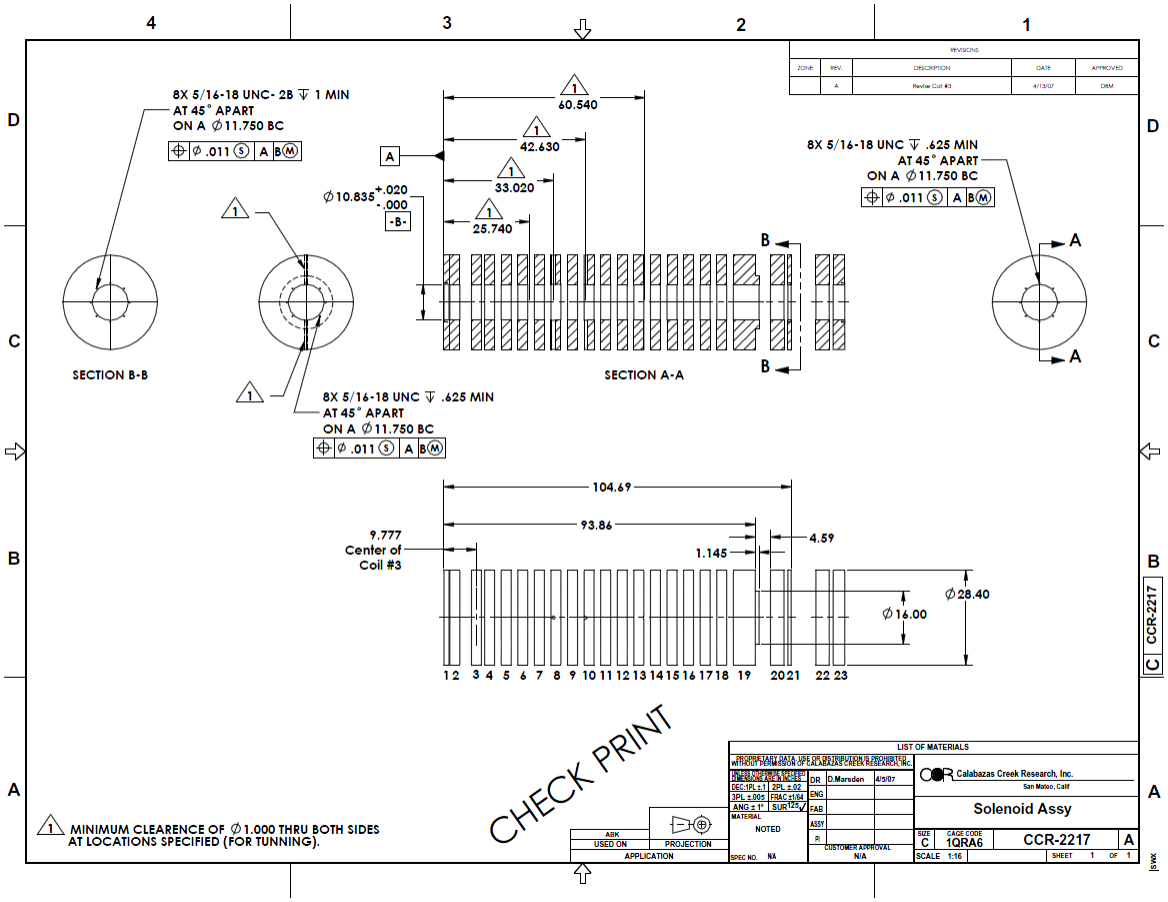

Figure 39. Design for the solenoid. Dimensions are in inches.

Conclusion

All of the components of the ABK, except for the solenoid, were completed. The cathode for the electron gun was run up to temperature, and all of the RF components were cold tested with satisfactory results. The tube was ready for final assembly and bakeout. However, as discussed in the Introduction, the program resources were expended at that point, and, given that there appeared to be no market for the tube, it was decided to terminate the program.

References

1. M. Friedman, et al., "Efficient Conversion of the Energy of Intense Relativistic Electron Beams into RF," Rev. Sci. Instrum. 61, 171 (1990).

2. M. Friedman, V. Serlin, M. Lampe, and R. Hubbard, "Intense Electron Beam Modulation by Inductively Loaded Wide Gaps for Relativistic Klystron Amplifiers," Phys. Rev. Lett. 74, 1214 (1995).

3. B. Carlsten, et al., Intense Space-Charge Beam Physics Relevant to Relativistic Klystron Amplifiers," IEEE Trans. Plasma Science, 22 (5) (1994)

4. M. Fazio, et al., "Progress Otward a Gigawatt-Class Annular Beam Klystron with a Thermionic Electron Gun," CP625, Proceedings of High Energy Density and High Power RF: 5th Workshop, B. Clarsten, ed. 159-168 (2002)

5. J Pasour, David Smithe, Larry Ludeking, and Moshe Friedman, "High Power, Annular-Beam Klystron Amplifier," High Energy Density and High Power RF: 5th Workshop, ed. B.E. Carlsten, 15 (2002).

6. R.True, "Beam optics calculations in very high power microwave tubes," Technical Digest., International Electron Devices Meeting, pp. 403-406 (1991).